NSRRC - J04662(2015)

ACS APPLIED MATERIALS & INTERFACES

Research Article

www.acsami.org

Nonvolatile Organic Field-Effect Transistors Memory Devices Using Supramolecular Block Copolymer/Functional Small Molecule Nanocomposite Electret

Hui-Yen Chi,[†] Han-Wen Hsu,[†] Shih-Huang Tung,*[,‡] and Cheng-Liang Liu*[,†]

[†]Department of Chemical and Materials Engineering, National Central University, Taoyuan, 32001 Taiwan

[‡]Institute of Polymer Science and Engineering, National Taiwan University, Taipei, 10617 Taiwan

Supporting Information

ABSTRACT: Organic field-effect transistors (OFETs) memory devices based on hybrid nanocomposite electret were fabricated by cooperative supramolecular polystyrene-*block*-poly(4-vinylpyridine) (PS-*b*-P4VP) with two different block compositions (asymmetric L1 and symmetric L2) that contain hydroxyl-functionalized ferrocene small molecules (FMs). Because of the selective hydrogen interaction between the hydroxyl groups of FM and pyridine groups in P4VP block, the small FMs can preferentially disperse in the P4VP nanodomain, which can be used as nanostructured charge-trapping nanocomposite electret (L1-FMX and L2-FMX) under solvent-annealing process. The charge-storage functionalities can be easily tailored by morphologies of the hybrid nanocomposite thin film and spatial distribution of the FM molecules in which the relative molecular mass of block copolymers and the FM loading ratio can further control both of them. These block copolymer nanocomposite thin film electrets with charge-controlling guest FM for OFETs memory devices exhibit significant features including the ternary bits storage, high-density trapping sites, charge-carrier trapping of both polarities (ambipolar trapping), and solution processing that can make important progress for future advanced storage and memory technology.

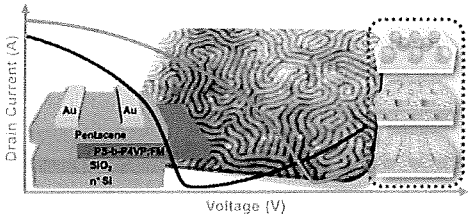

KEYWORDS: *nonvolatile memory, block copolymer, nanocomposite, supramolecular, organic field effect transistor*

INTRODUCTION

Organic field-effect transistors (OFETs) have multifunctionalities for a broad range of use in radio frequency identification (RFID) tags, sensors, electronic papers, memory devices, etc.[1−7] Among all these important developments, organic/polymeric memory devices based on OFETs architecture is one of the emerging/potential technology for information storage media.[8−16] Typically, OFETs memories have been classified into three main categories based on the charge storage and polarization methods of the dielectric layer:[8−11] floating-gate memory, chargeable electret memory, and ferroelectric memory. Among these, an electret is a dielectric material that has a quasi-permanent electric charge for storage.[17−27] As a result, polymeric electret as a charge-trapping layer is inserted into the OFETs that has been applied to storage of data in nondestructive readout operation. Sequence of one or more voltage pulses/sweeps in gate electrode are used to evoke the digital signals indicative of nonvolatile state of OFETs memory cell. In general, single polymer-based electret materials that demonstrate the hysteresis behavior include pendent polymers[17−19] and donor−acceptor polyimides[23−25] utilized as charge storage layer, mainly concerned with manipulating polymer structures for correlation to the memory properties. The hybrid polymer nanocomposite electret comprising functional small molecules[26−28] or carbon-based materials[21,29] guest fillers in the polymer matrix can also be selected to control memory properties via the intrinsic nature of additives and their loading concentration.

The conventional flash memory that stores information in an array of memory cells made from floating-gate transistor remains in the lead of the nonvolatile memory market. However, facing the device scaling-down problem in the near future, the requirements of high charge-storage capacity and long retention are still a critical challenge. In this case, nanostructured materials play a critical role in serving as the charge-storage sites of the transistor-type memory.[10,15] For fulfilling this goal, self-organizing block copolymers thin film provides a straightforward means for achieving small feature size and high densities in continuous progress of electronics industry.[30] Microphase-separated nanostructures of block copolymers spontaneously form a regular arrangement and extended internal interfaces between the covalently linked incompatible block. Supramolecular approach particularly based on the addition of functional small organic molecules or metal nanoparticles (NPs) that selectively bond to one block of block copolymers in a noncovalent form can be essential to govern the dimensional scaling issue to the smaller sizes necessary for utilization by memory technology generation.[26,29,31−41] Wei's

Received: September 28, 2014
Accepted: February 25, 2015
Published: February 25, 2015

 © 2015 American Chemical Society

DOI: 10.1021/acsami.5b00338
ACS Appl. Mater. Interfaces 2015, 7, 5663−5673

and Watkins's group have fabricated nonvolatile OFETs memory devices featuring diblock copolymers layer incorporating metal NPs that enables tunable memory characteristics and extendable high density of charge-trapping memory.[40,41] Recently, Chen's group also reported sugar-based block copolymers supramolecules with pyrene molecules for enhancing memory properties.[26] Such regular block copolymer microdomains can be used as host structures for incorporation of these additives with chemical affinity and geometry suitable to influence additives spatial organization. The key issue from the ability to selectively position additives in the target block copolymers domains and control the final nanocomposite morphology still needs to be considered for innovation applications in future nonvolatile OFETs memories.

In this study, block copolymers nanocomposite electret thin films through supramolecular approach and their application for OFETs memory devices were reported. Redox-active ferrocene molecule intrinsically can exhibit distinct charged or discharged states, which can represent the logical ON and OFF states.[42] Therefore, two different weight ratios were used in constituent blocks of polystyrene-*block*-poly(4-vinylpyridine) (PS-*b*-P4VP; L1 and L2) as a model substrate with which functional small molecules of ferrocenemethanol (FM) were associated by hydrogen bonding to the vinylpyridine group in various loading concentrations, as shown in Figure 1. Exposure of block

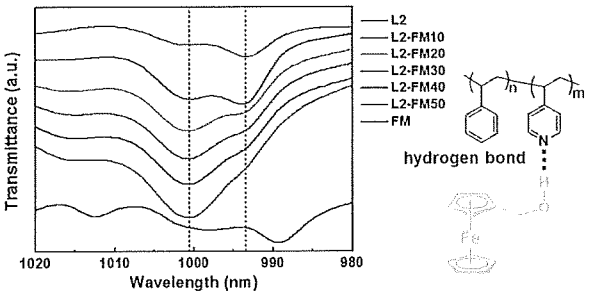

Figure 1. Schematic illustration and FTIR spectrum of PS-*b*-P4VP:FM nanocomposite thin film.

copolymers nanocomposite thin films to the solvent vapor atmosphere can provide the versatility of achievable morphological states. The morphology of the nanocomposite thin films, the loading of the FM, and the utility of these for obtaining desirable memory device properties were emphasized. Morphology-induced modulation of electrical memory behaviors can be related to the positioning of incorporated FM small molecules within PS-*b*-P4VP matrix. The formation of high density and high bit nonvolatile OFETs memories will potentially be upgraded and control the device performance.

EXPERIMETAL SECTION

Materials. Two linear PS-*b*-P4VP block copolymers, denoted as L1 and L2 (M_n(PS) = 24 000 g mol^{-1}, M_n(P4VP) = 9500 g mol^{-1}; M_w/M_n = 1.10 for L1; M_n(PS) = 20 000 g mol^{-1}, M_n(P4VP) = 17 000 g mol^{-1}; M_w/M_n = 1.08 for L2), respectively, from Polymer Source, Inc. (Canada) were used as received. Ferrocenemethanol (FM) from Acros (USA) and pentacene from Lumtec (Taiwan) were obtained without further purification. The solvents, such as chloroform ($CHCl_3$) and tetrahydrofuran (THF), were purchased from Sigma-Aldrich (USA) of the anhydrous grade.

Preparation of Supramolecular Block Copolymer Nanocomposite Thin Films. The linear PS-*b*-P4VP block copolymer (L1 or L2) hybrid solutions were prepared by dissolving suitable amounts of copolymer powder and accurately weighting required amounts of FM in an appropriate volume of $CHCl_3$ separately to achieve a concentration of 8 mg mL^{-1}. All the blend solutions were obtained by dropwisely adding appropriate volume of FM in $CHCl_3$ to the block copolymer solutions (FM content ranging from 0 wt % to 50 wt % relative to block copolymers amount) and stirred for 7 d at room temperature to allow for the formation of hydrogen bonds. A substrate of 300 nm SiO_2/heavily doped n-type Si was cleaned by ultrasonic bath of the following order of solvent each for 10 min: deionized water, acetone, and isopropanol. All the pristine block copolymers and hybrid nanocomposites were fabricated as thin films by spin coating the corresponding solutions onto precleaned substrate at 2500 rpm for 60 s and then dried, resulting in a ca. 40−50 nm thick thin film. These nanocomposite thin films were coded as L1-FMX or L2-FMX, where X represents the weight fraction of FM in L1 or L2:FM hybrids. Thin-film samples were then exposed in a screw-tipped jar to saturated THF vapors kept at room temperature for different times (8 h for L1-FMX and 12 h for L2-FMX thin films, respectively). After solvent annealing, the nanocomposite thin films were dried to remove the residual solvent. Table 1 summarizes characteristics of all hybrids prepared in this work. All the sampling procedures in film states were obtained under N_2-filled glovebox.

Characterization. Fourier transform infrared (FTIR) spectroscopy (PerkinElmer Spectrum One) was conducted to identify the hydrogen-bonding interaction in hybrid nanocomposite thin film between hydroxyl group on FM and pyridine group in P4VP block. The thickness of block polymer nanocomposite film was measured with DEKTAK 150 Surface Profilometer (Veeco). Atomic force microscopy (AFM) was performed in tapping mode at room temperature by Seiko SPA400 for which NANOSENSORS Si tips with a resonant frequency of 160 kHz were used. Grazing incident small-angle X-ray scattering (GISAXS) was performed at room temperature on the beamline BL23A in the National Synchrotron Radiation Research Center (NSRRC), Taiwan.

Organic Field-Effect Transistors Memory Device Fabrication and Measurement. After the PS-*b*-P4VP:FM nanocomposite thin films were deposited on the SiO_2/Si substrate to achieve the good formation of specific supramolecular nanostructures under solvent annealing, the active semiconducting pentacene channel was thermally deposited under a pressure of 5×10^{-6} Torr and a rate of 0.1 Å s^{-1}. Then the 50 nm thick Au source and drain electrodes were defined through a regular shadow mask with a channel length (L) and width (W) of 50 and 1000 μm, respectively. The electrical transport properties of the devices were recorded by probe station with Keithley 4200-SCS semiconductor parameter analyzer. Bottom-gate top-contact (BGTC) OFETs memories were adopted. All the fabrications and measurements were done under N_2-filled glovebox.

RESULTS AND DISCUSSION

The incorporation of functional small molecules into a specific location of phase-separated nanostructures enables the block copolymer nanocomposite with prominent features.[43−47] The supramolecule (L1-FMX and L2-FMX) is comprised of PS-*b*-P4VP (L1 or L2) with the P4VP block hydrogen-bonded to the FM small molecules, as illustrated in Figure 1. Spin-coated thin films from a nonpolar solvent of $CHCl_3$ were prepared, followed by solvent annealing for a sufficient time. The molecular design of supramolecular compounds and careful solvent annealing procedure can result in the selective incorporation of FM small molecules into a P4VP phase of block copolymer as well as the formation of uniform and specific morphology observed in L1-FMX and L2-FMX nanocomposite thin film in which FM behaves as a filler inside the L1 or L2 block copolymer matrix. Here, L2-FMX series was used as a representative for supramolecular hybrid characterization based on FTIR measurement. Figure 1 compares FTIR spectra of the 980−1020 cm^{-1} region for neat L2, neat FM, and

DOI: 10.1021/acsami.5b00338
ACS Appl. Mater. Interfaces 2015, 7, 5663−5673

Table 1. L1-FMX and L2-FMX Nanocomposite Electret and Their OFETs Device Performance

sample	$f_{PS}:f_{P4VP}:X^a$	$R_0{}^b$	morphology[c]	roughness (nm)	D (nm)	mobility ($cm^2\ V^{-1}\ s^{-1}$)	ON/OFF ratio	memory window (V)	
L1	72:28:0	0	S_{P4VP}	1.04	25.6	0.44	2.2×10^7	±60	1.3
								±80	5.0
								±100	20.8
L1-FM10	64:26:10	0.19	$S_{P4VP(FM)}$	0.90	26.4	0.34	2.9×10^7	±60	4.6
								±80	10.4
								±100	30.8
L1-FM20	57:23:20	0.44	$S_{P4VP(FM)}$	0.84	26.9	0.24	3.7×10^7	±60	4.0
								±80	15.3
								±100	42.5
L1-FM30	50:20:30	0.72	$C_{P4VP(FM)}$	0.94	36.3	0.36	9.0×10^6	±60	7.9
								±80	20.1
								±100	47.2
L1-FM40	43:17:40	1	PL	0.96	30.0	0.37	6.4×10^6	±60	5.5
								±80	17.8
								±100	45.8
L2	54:46:0	0	C_{P4VP}	1.02	36.3	0.27	1.7×10^7	±60	1.9
								±80	5.7
								±100	21.3
L2-FM10	49:41:10	0.12	$C_{P4VP(FM)}$	0.92	37.2	0.38	2.6×10^7	±60	5.1
								±80	15.4
								±100	34.4
L2-FM20	43:37:20	0.27	$C_{P4VP(FM)}$	0.89	37.2	0.32	4.5×10^7	±60	5.5
								±80	26.7
								±100	46.3
L2-FM30	38:32:30	0.45	PL	0.91	30.5	0.30	1.1×10^7	±60	6.4
								±80	18.6
								±100	42.3
L2-FM40	32:28:40	0.71	C_{PS}	0.93	35.0	0.26	7.7×10^6	±60	10.9
								±80	32.7
								±100	66.9
L2-FM50	27:23:50	1	C_{PS}	1.18	37.2	0.17	2.7×10^8	±60	20.8
								±80	44.3
								±100	78.4

[a]Weight fraction between PS:P4VP:FM. [b]Stoichiometric ratio of hydroxy to pyridine groups. [c]S: sphere, C: cylinder, PL: perforated lamella.

L2-FMX nanocomposite thin films. The FTIR spectra support hydrogen bonding between pyridine groups on P4VP block and hydroxyl groups on FM, where the absorbance at 993 cm^{-1}, which belongs to free pyridine, decreases (absence from FM spectrum) and the absorbance at 1001 cm^{-1}, which indicates the hydrogen-bonded pyridine, increases with loading ratio of FM additive. Besides, the quasi-disappearance of the 993 cm^{-1} free pyridine band in L2-FM50 indicates that the extent of FM/P4VP hydrogen bonding in this equimolar blend is close to complete, consistent with the estimated stoichiometric ratio of hydroxy to pyridine groups (in this case, $R_0 = 1$ in Table 1).

AFM images of neat L1 or L2 and the nanocomposite thin films after annealing in THF vapor are shown in Figures 2 and 3. The thicknesses of the thin films are 40–50 nm, determined by a surface profiler. Pristine L1 and L2 block copolymers exhibit different morphologies, depending on the weight fraction (f) of two blocks. In L1 thin film, dotlike nanodomains were clearly evidenced (Figure 2a), in agreement with previously reported results from the similar nonsymmetric system.[48] With P4VP weight fraction (f_{P4VP}) of 28% in neat L1, P4VP domains are supposed to be cylindrical. However, since THF is a selective solvent to PS and may preferentially swell PS domains during solvent annealing, the dot morphology should be composed of P4VP spheres surrounded by PS matrix after fast evaporation of THF. The morphologies of the L1-FMX composite thin films can be significantly tailored by varying the FM loading ratio, as shown in Figure 2b–d. At a low amount of FM ($X \leq 20\%$), L1-FMX thin films exhibit dotlike patterns similar to those of neat L1. The amount of added FM in these cases is insufficient to change the structure, and thus the films maintain P4VP(FM) spheres in PS matrix. As X is increased to 30%, the AFM image shows fingerprint-like pattern with long and wandering domains, which are P4VP(FM) cylinders lying on the substrate due to the increase of P4VP(FM) fraction. Further increasing X to 40% in L1 hybrids, a dotlike pattern is seen again. Since the fraction of P4VP(FM) has been as high as 57%, the dot pattern should not reflect a spherical nanostructure. Instead, it is more likely that such a pattern is caused by a perforated lamellar structure, and the dots are the perpendicular PS cylindrical domains in one of the layers, as illustrated in Figure 2e. In neat L2 case, a fingerprint-like pattern was observed in thin film, as shown in Figure 3a. The symmetric L2 theoretically tends to form lamellar structures, but due to the swelling of PS domains in THF vapor, P4VP self-organizes into cylinders in PS matrix, and the cylinders are parallel to the surface, thus forming the fingerprint-like pattern. When X is below 20%, L2-FMX thin films maintain a fingerprint-like pattern (Figure 2b,c). At X = 30%, the structure

DOI: 10.1021/acsami.5b00338
ACS Appl. Mater. Interfaces 2015, 7, 5663–5673

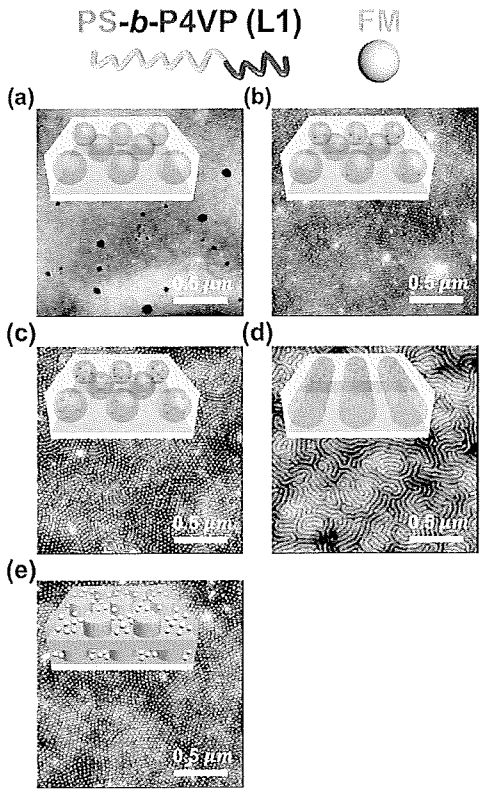

Figure 2. AFM images and schematic illustration of proposed morphologies of the L1-FMX electret thin film after solvent annealing: (a) L1, (b) L1-FM10, (c) L1-FM20, (d) L1-FM30, and (e) L1-FM40 nanocomposite electret.

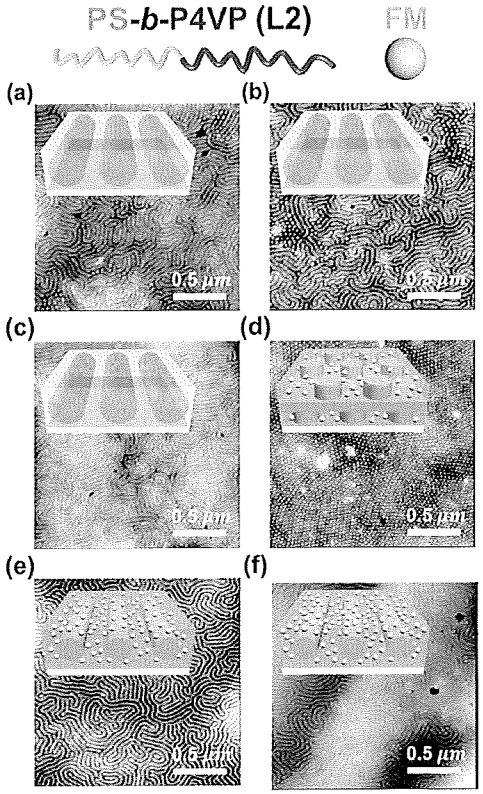

Figure 3. AFM images and schematic illustration of proposed morphologies of the L2-FMX electret thin film after solvent annealing: (a) L2, (b) L2-FM10, (c) L2-FM20, (d) L2-FM30, (e) L2-FM40, and (f) L2-FM50 nanocomposite electret.

is transformed to perforated lamellae with perpendicular PS cylinders in P4VP(FM) matrix on top of the film (Figure 2d). At X above 40%, fingerprint-like patterns appear again (Figure 2e,f), and it is highly possible that the PS blocks now form parallel cylinders in P4VP(FM) matrix because at this high fraction of P4VP(FM), PS blocks become minor phase. In sum, a series of structures induced by the fraction of P4VP(FM) due to the selective incorporation of FM into a P4VP phase via hydrogen bonding can be produced, including P4VP(FM) spheres and cylinders, perforated lamella, and PS cylinders. It is also noticed that no significant macrophase aggregation of FM occurs from these supramolecular systems, implying that FM molecules can be retained in P4VP phase through hydrogen bonding even at X values as high as 50%.

GISAXS was conducted to acquire the quantitative data of morphologies for the supramolecular thin films. Figures S1a,c,e,g,i and S2a,c,e,g,i,k of Supporting Information show the two-dimensional (2D) GISAXS patterns of L1-FMX and L2-FMX thin films annealed in THF for 8 and 12 h, respectively. In addition, the in-plane profiles of q_y scan extracted at q_z = 0.165 Å^{-1} were demonstrated in Figures S1b,d,f,h,j and S2b,d,f,h,j,l of Supporting Information. Domain spacing (D) can be estimated from scattering vector at first-order peak, and the calculated D is summarized in Table 1. For L1-FMX-based thin films, the spacing of sphere-forming samples (X ≤ 20%) is 25–27 nm. When the parallel P4VP(FM) cylinders are formed at X = 30%, the spacing greatly increases to 36.3 nm. At X = 40%, the spacing of the perpendicular PS cylinders in perforated lamellae does not keep increasing but instead drops to 30.0 nm. The larger spacing for parallel cylinders is because the film is so thin that only 1–2 cylinder layers are contained in the film where the spatial arrangement of the parallel cylinders is analogous to that of perpendicular lamellae. The spacing estimated from the first-order diffraction peak is thus the center-to-center distance between cylinders, which is larger than the real spacing of hexagonally packed spheres or cylinders. A similar trend was observed in L2-FMX-based nanocomposite thin films. The spacings of parallel cylinders, whether P4VP(FM) or PS, are in the range of 35–37 nm, while that of perpendicular PS cylinders in perforated lamellae (X = 30%) is smaller, ~30.5 nm. As described below, the varying morphologies caused by the addition of FM are found to greatly affect the electrical memory properties.

The block copolymer nanocomposite electrets based on L1-FMX and L2-FMX were fabricated for nonvolatile memory devices applications. The electrical properties were studied using pentacene-based BGTC OFETs device architectures. The output characteristics for OFETs devices including pristine block copolymer and nanocomposite electret under various V_g in steps of 2 V are shown in Figure S3 of Supporting Information. The shapes of I_d–V_d curves closely resemble the output characteristics of conventional p-type transistor, exhibiting a linear region at low V_g and a saturation region at high V_g. To confirm the memory effect from the electret layer, cyclic transfer curves over distinct gate voltage ranges were

DOI: 10.1021/acsami.5b00338
ACS Appl. Mater. Interfaces 2015, 7, 5663–5673

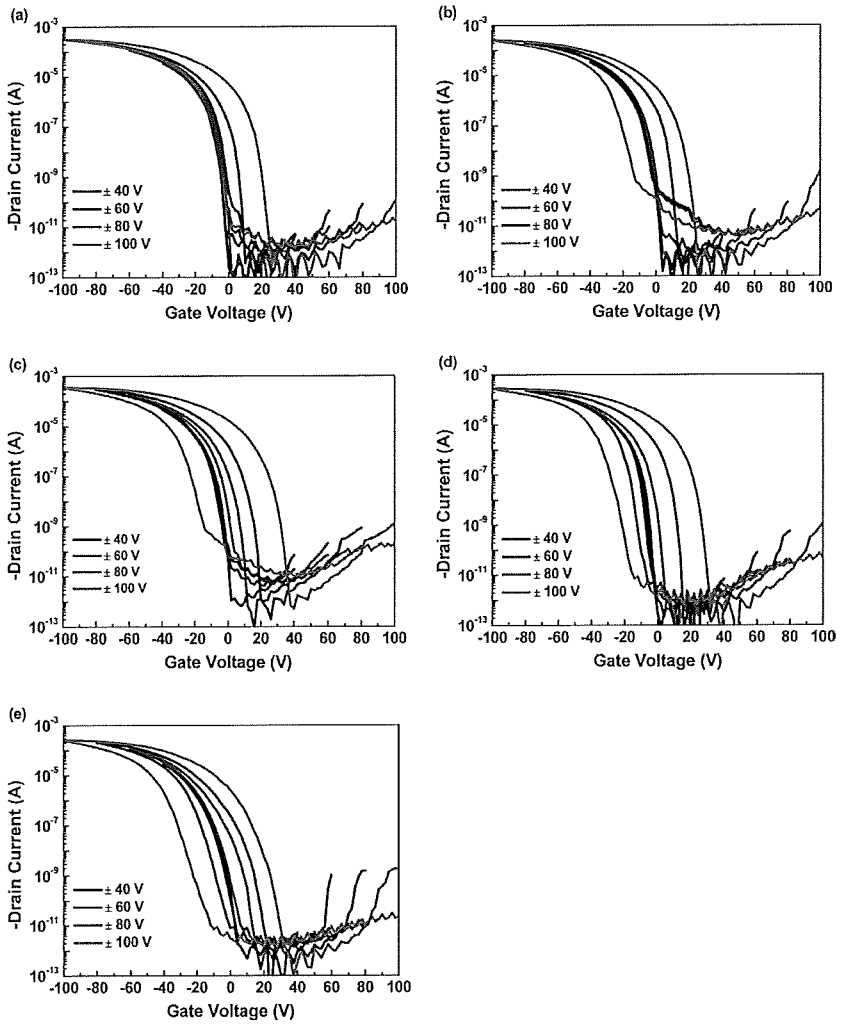

Figure 4. Cyclic transfer curves from OFETs memory devices based on (a) L1, (b) L1-FM10, (c) L1-FM20, (d) L1-FM30, and (e) L1-FM40 electret under different V_g scan ranges of ±40, ± 60, ± 80, and ±100 V, respectively.

tested. All the I_d–V_g transfer characteristics of the OFETs memory devices (Figures 4 and 5 for in L1-FMX and L2-FMX hybrid electret devices, respectively) show current modulation at a forward sweep from positive to negative V_g as well as a fixed V_d of −50 V, and the devices exhibit the saturated field-effect mobility based on transistor standard models of ~0.17–0.44 $cm^2 V^{-1} s^{-1}$ with an ON/OFF current ratio of more than 1 × 10^7 in average from 10 independent samples using the same process. The additional hybrid electret layers do not degrade the OFETs devices performance due to the similar crystal growth size of deposited pentacene grain, as shown in Figure S4 of Supporting Information. Then the typical counterclockwise current hysteresis was observed with a memory window, defined as threshold voltage shift between these two scans, when the device was subsequently swept backward from negative to positive V_g. The memory windows of the hysteresis loops under various sweeping ranges are summarized in Table 1. As noted, all the memory windows in L1-FMX and L2-FMX nanocomposite electret devices continuously increase proportionally to counterclockwise sweeping range amplitude. Nearly hysteresis-free OFETs memory device operation was detected when V_g sweep less than ±40 V was used. It can be seen here for pristine block copolymer electret-based device that during the V_g sweep from −60 (−80 or −100) V to 60 (80 or 100) V the initial transfer curves were shifted only in a positive direction by 1.3 (5.0 or 20.8) V for L1 electret and 1.9 (5.7 or 21.3) V for L2 electret, as shown in Figures 4a and 5a. The hysteresis loops suggest that the memory characteristics of pristine block copolymer electret-based OFETs memories are due to the electron trapping by hydrophilic electron-enriched P4VP domain of the PS matrix in the L1 or L2 layer that is similar to the previous results published by Wei's group.[22] When the pristine block copolymer electret is charged at more positive voltage bias, a higher number of charge carriers (electron) accumulate, and electrostatic potential of the trapped charge also increases. However, the shifted transfer curves move back to the initial position after the reverse sweep, and the chargeable electret are now discharged again. For hybrid nanocomposite electret-based device, the memory window and trapped/dissipated charges increase almost linearly with V_g sweeping ranges, as evidenced in Figures 4b–e and 5b–4f. In the case of L1-FMX series nanocomposite electrets, the

DOI: 10.1021/acsami.5b00338
ACS Appl. Mater. Interfaces 2015, 7, 5663–5673

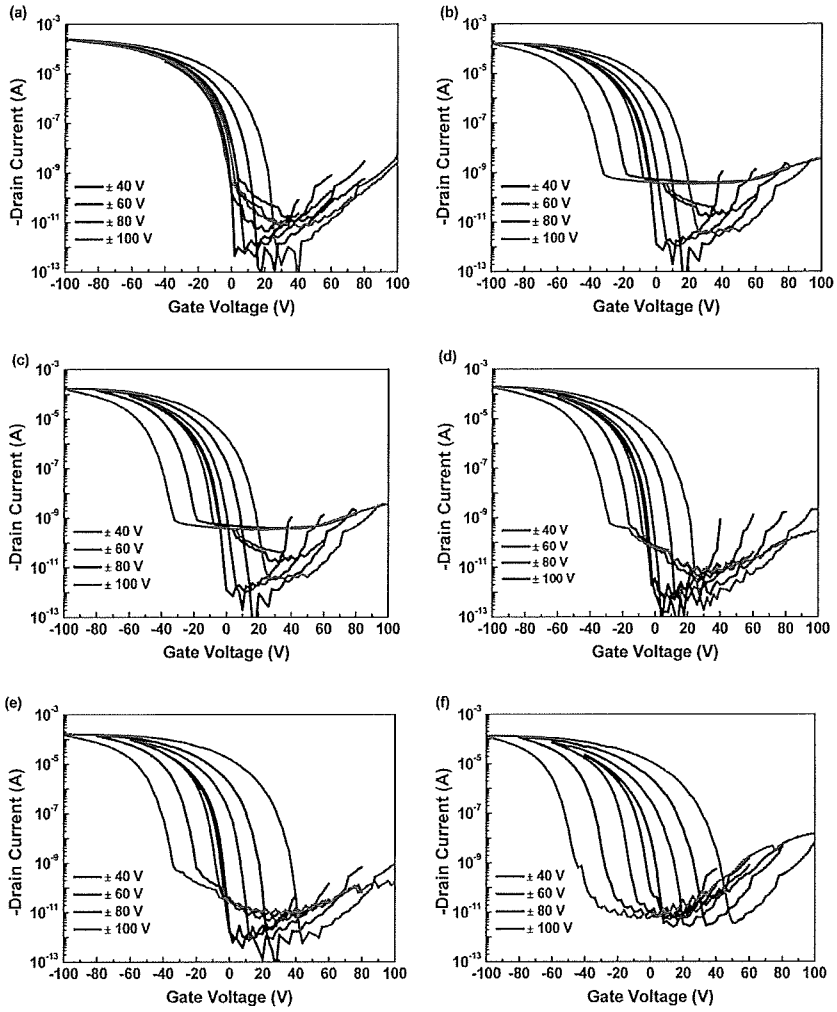

Figure 5. Cyclic transfer curves from OFETs memory devices based on (a) L2, (b) L2-FM10, (c) L2-FM20, (d) L2-FM30, (e) L2-FM40, and (f) L2-FM50 electret under different V_g scan ranges of ±40, ± 60, ± 80, and ±100 V, respectively.

hysteresis window increases to 30.8 and 42.5 V for L1-FM10 and L1-FM20, respectively, under ±100 sweeping range and based on morphologies of spherical P4VP(FM) in the PS matrix (same as L1 morphology). When 72% of FM molecules were presented in the P4VP (cylindrical L1-FM30 nanocomposite electret), additional charge trapping by these FM sites further broadens the memory window to 47.2 V. In contrast, L1-FM40 hybrid electret (100% of FM attached on the P4VP) with a perforated lamellar phase slightly deteriorates the memory window. Similar trend in memory window can be discovered in the L2-FMX series devices: increase from L2-FM10 to L2-FM20 device (same as parallel cylindrical L2 morphology), then decrease in perforated lamellar of L2-FM30 hybrid electret, and finally continuous increase from L2-FM40 to L2-FM50 device again (both are PS cylinder microdomains). Among all, the L1-FM30 and L2-FM50 device exhibit largest memory window of 47.2 and 78.4 V in L1-FMX and L2-FMX series, respectively, during applied V_g of ±100 V. An interesting point here is that the V_{th} in forward and reverse curves are shifted to a more positive and negative region, respectively, indicating that the combined effects caused by both electron and hole trapping (or so-called "ambipolar trapping") ability can strength the memory properties.[49−51] It also suggests that hydrogen-bonded FM molecules into the L1 or L2 as hybrid nanocomposite electret can effectively generate the hole (majority carrier) and electron (minority carrier) trapping capability since partial negative charge trapping can be originated from neat L1 or L2 block copolymer electret under electrical field.

To further confirm the effective control over the hybrid nanocomposite electret, the statistical variations in the memory ratio value of the OFETs memory devices containing L1-FMX or L2-FMX electret layer are shown in Figure S5 of Supporting Information. Neat L1 and L2 block copolymer electret devices have similarly programmable/erasable memory window, but the hybrid electrets devices after blending with FM small molecules have an enhanced memory window since the nanocomposite morphologies as well as loading ratio and spatial position of FM additives can change the memory characteristics. An increase in FM concentration in the hybrid electret can widen the hysteresis window at a fixed morphology (for sphere between L1, L1-FM10 and L1-FM20, for P4VP(FM) cylinders between L2, L2-FM10 and L2-FM20, and for PS cylinders between L1-FM40 and L2-FM50), thus indicating the occurrence of

DOI: 10.1021/acsami.5b00338
ACS Appl. Mater. Interfaces 2015, 7, 5663−5673

stronger carrier trapping with higher loading of the FM molecules. High spatial density of FM molecules in the P4VP domain or entire film and small intermoleculear distance as the FM loading ratio increases should create a much higher probability of trapping the charge. The memory behavior of the block copolymer nanocomposite electret-based OFETs memory devices can also be directly corrected with their nanostructures. At a fixed and low FM loading range, a well-defined cylindrical L2-FM10 (or L2-FM20) electret oriented in the film plane displays a more active physical route for charge trapping relative to the observed L1-FM10 (or L1-FM20) electret attributed to the spherical P4VP(FM) cylinder domains in the insulating PS matrix. In such a confined cylindrical geometry based on L2-FM10 (or L2-FM20) device, effectual charge trapping occurred in the interface layer between pentacene and hybrid electret triggers larger memory window due to the increase in interfacial area for charge trapping in P4VP(FM) domains.[26] However, in the case for high-loading range, the memory window of the devices based on perforated lamellae in L1-FM40 and L2-FM30 electret declined to 45.8 and 42.3 V, which is smaller than that of the hybrid electret at same loading with the fingerprint pattern for L2-FM40 (66.9 V) and L1-FM30 (47.2 V). It can primarily be summarized that in the nanocomposite electret with a fixed FM loading concentration but different morphologies, perhaps the standing perforated lamellar phase in L1FM40 or L2-FM30 are not able to perfectly be charging the traps across the horizontally oriented PS lamellae where the PS block and its phase can act as a barrier for charge transport/trap through the block copolymer nanocomposite film layer[52−54] even though these devices contain a higher FM loading concentration. Accordingly, the specific morphology from the hybrid electret composed of perforated lamellae normal to the substrate direction mainly accounts for the decreased memory window from deteriorated ability for maintaining the trapping charge in P4VP(FM) nanodomain. The fingerprint morphological pattern (parallel cylinders) in the hybrid nanocomposite electret can have a structural advantage to store the charges efficiently without loss, and the bit density of storage can be easily increased at higher P4VP loading. These results suggest that the memory properties in our OFETs memories are significantly altered with FM additives. As a result, the supramolecular nanocomposites open a way to tailor the memory hysteresis by morphology-manipulatable charge-trapping sites (from block ratio of copolymers and FM loading ratio), thereby meeting the high performance requirement for potentially practical applications.

The counterclockwise hysteresis loop mentioned above can be used for OFETs memory devices, and the V_{th} shift by trapping the charges in the hybrid electret film leads to modulate I_d of each logic state in a memory device. The nonvolatile and reversible memory characteristics were also determined by electrical pulses. As shown in Figure 6a, the initial transfer curve of OFETs memory devices based on L2-FM50 electret is affected by V_g with duration of 1 ms. The device shows a negative shift of the transfer curve relative to initial curve according to the V_g of −80 V (route (i)); this set of conditions is referred to as hole-erasing (E^h) state since the resultant I_d is below the initial I_d value. Meanwhile, positive V_g pulse (= 70 V) causes a positive shift of the transfer curve to the initial position (route (ii)) as hole-programming state (P^h). As the applied positive voltage increases to 80 V, the amount of positive shift increases (route (iii)). This V_{th} change by parallel

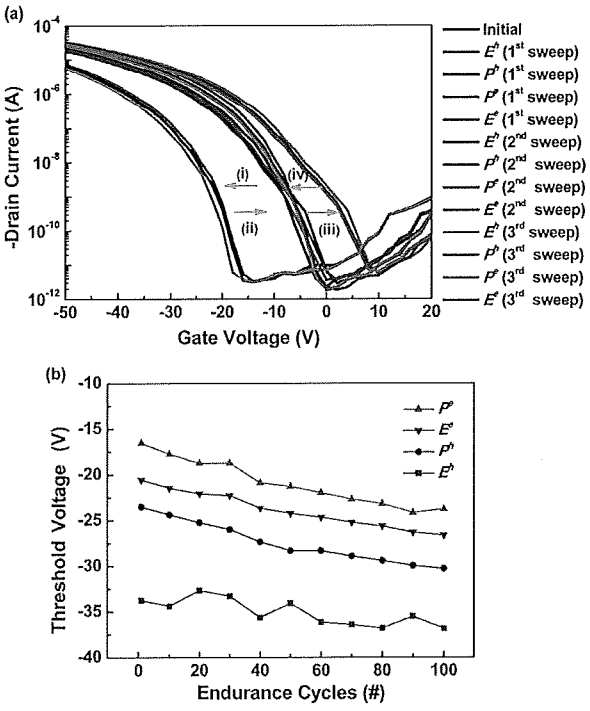

Figure 6. (a) Transfer curve scans after the E^h, P^h, P^e, and E^e pulses, respectively, as one test pulse sequence for endurance test. (It shows the transfer curve scan during three continuous cycles in this figure.) (b) Multiple endurance characteristics established in the OFETs memory devices based on L2-FM50 nanocomposite electret as a function of bias cycles. The threshold voltage was measured in every 10 endurance cycles after repeating the $E^h/P^h/P^e/E^e$ pulse with continuous bias pulses of −80/70/80/−50 V for 1 ms.

shift of the transfer curves indicates that the positive electrical pulse generates a certain amount of effective negative charges in P4VP(FM) (as electron-programming (P^e) state). Finally, the charging state can return to the initial state (route (iv)) by applying V_g of −50 V (as electron-erasing (E^e) state). All these transfer curve shifts are thus collectively referred to as one complete scan between these E^h, P^h, P^e, and E^e states. Figure 6a displays three continuous complete scans after the E^h, P^h, P^e, and E^e pulse, and the transfer curves of block copolymer nanocomposite electret devices can still return to the initial position after utilizing these positive/negative electrical pulses. A typical device multiple data endurance test is performed in Figure 6b with V_{th} measuring obtained from transfer curve scan after controllably repeating $E^h/P^h/P^e/E^e$ pulse operation. During this test, the V_d value was set as −50 V, and V_g pulses with 1 ms were applied to charge-trapping operation between pentacene channel and hybrid electret layer. Only slight decay of V_{th} between these four states was observed for at least 100 cycles. Figure 7 shows the retainability, that is, retention time for the stored data in the hybrid electret OFETs memory devices. The reliability of OFETs memories was examined by data retention of four independent states. The memory device from L2-FM50 electret is retained after E^h operation of −80 V, V_g, P^h operation of 70 V, V_g, P^e operation of 80 V, V_g, E^e operation of −50 V, V_g for 1 ms, and then the I_d response at a low reading V_g of −5 V is measured with time in a controllable manner. Distinguishable current separation between low I_d level ($\sim 5 \times 10^{-11}$ A) for E^h state, intermediate I_d level ($1 \times 10^{-10} \sim 1$

DOI: 10.1021/acsami.5b00338
ACS Appl. Mater. Interfaces 2015, 7, 5663−5673

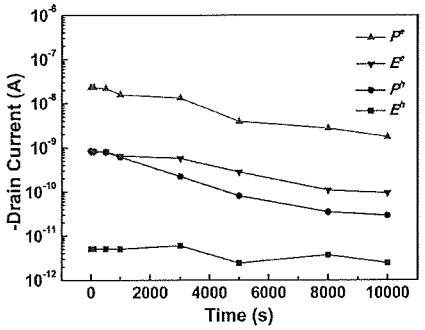

Figure 7. Memory-retention characteristics of the OFETs memory device based on L2-FM50 electret. The devices were initially operated under E^h, P^h, P^e, and E^e conditions by setting the V_g pulse of −80, 70, 80, −50 V, respectively, for 1 ms.

$\times 10^{-9}$A) for P^h and E^e states (same I_d level with initial state), and high I_d level ($\sim 1 \times 10^{-8}$ A) for P^e state is reliably measured in terms of nondestructive readout for 1×10^4 s, and thus detected tristable states of nonvolatile memory can be observed via retentively reading the I_d as a function of V_g pulse. Therefore, both retention time and endurance repeatability characteristics reveal that OFETs with an additional nanocomposite thin film electret can be successfully used for nonvolatile memory applications.

We already demonstrated that OFETs with hybrid electret materials can be used for memory applications. The shifts in V_{th} in response to the different V_g sweep ranges or pulses are clearly visible in the device transfer characteristics. Such memory characteristic is proposed to result from the charge balance between the electret layer and organic semiconducting channel (pentacene) under the applied V_g, as shown in Figure 8, and the switching mechanism for OFETs memories can be explained by electric field-induced charge-carrier trapping in the electret. The flat-band energy diagram of OFET memories is shown as a function of spatial dimension in Figure 8a. No charge carriers exist or transfer in the semiconductor layer in the absence of external electric field. Upon application of a large negative V_g pulse (Figure 8b), the observed negative shift in V_{th} for E^h reflects positive charging in the electret, which is attributed to the suitable highest occupied molecular orbital (HOMO) level that allows holes to pass through the block copolymer matrix and to be trapped in the FM units. When a positive V_g pulse is applied (Figure 8c), holes are expelled from the trapping sites or recombined with the electrons transferred from pentacene, corresponding to P^h that functions as discharging of stored information. In the case of applying a large positive V_g pulse (Figure 8d), both FM and electron-accepting P4VP facilitate the trapping of the electrons that tunnel the PS barrier layer from negatively charged pentacene into the low-lying lowest unoccupied molecular orbital (LUMO) of P4VP(FM) and cause a positive shift in V_{th} although FM has a higher LUMO energy level. The following

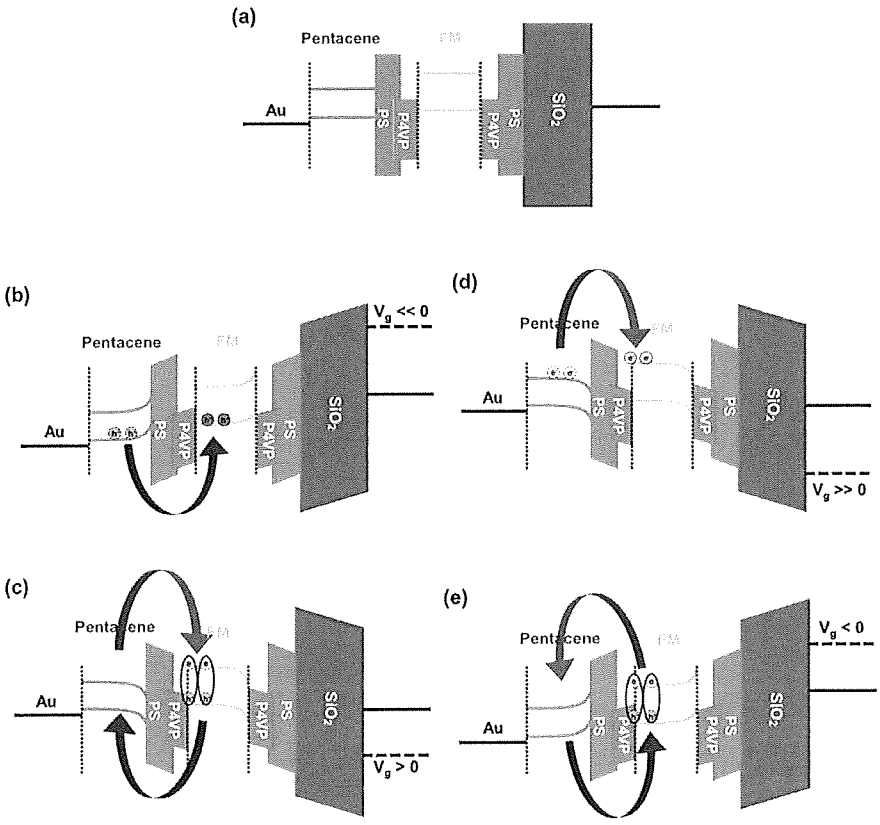

Figure 8. Switching mechanism illustration of the energy-band structures of the OFETs memory devices using hybrid nanocomposite electret. (a) Initial condition and under (b) E^h, (c) P^h, (d) P^e, and (e) E^e processes.

DOI: 10.1021/acsami.5b00338
ACS Appl. Mater. Interfaces 2015, 7, 5663−5673

negative V_g pulse can then lead to an E^e due to the detrapping of the electrons from P4VP(FM) or recombination of the hole from pentacene as illustrated in Figure 8e. Such trapping/detrapping processes from bipolar charges result in the bidirectional shifts in V_{th} (both positive and negative directions) as long as V_g pulse/bias is large enough to widen the memory window. It is suggested that the matching of HOMO/LUMO levels of the host polymer and small molecules is critical for such devices to show memory characteristic. Furthermore, L1 and L2 block copolymer acts as a template for defining the FM nanoscaled trapping sites so that the nanocomposites are able to form effective electrets for memory devices. Among the varying nanocomposites, it is apparent that the parallel-oriented cylindrical morphology at higher FM loading concentration is more capable of trapping charges, while it still maintains the uniformity of trapping density across the device area as well as the reliability and reproducibility in memory device performance.

We summarize here memory device performance benefits derived from controlling the nanostructured chargeable electret using supramolecular hybrid block copolymers nanocomposites as follows: (1) The presence of charge storage in hybrid electret determines a reversible shift in V_{th}, possibly enabling a ternary data storage device. The achievement on increase in number of memory states of each memory cell can increase data storage without decreasing the memory cell size to overcome the difficulties of scaling-down problem. (2) Device nonvolatility is ensured by using P4VP(FM) trapping sites electrically isolated by thick enough PS insulator to prevent current leakage and applicability of hybrid nanocomposite thin film for addressing prototype devices in which the density and spatial confinement of charge-trapping sites are controllably defined by bottom-up supramolecular strategies, usefully scaling to higher densities extremely well. Pretty high concentration of FM as multiple trapping molecules can be loaded in block copolymers due to the hydrogen-bonded interaction. (3) Ambipolar trapping characteristics governed by energy-level alignment across the interface between the active layer materials, charge trapping electret, and electrode found in the present OFETs memories can further enlarge the memory window as well as increase the storage capacity. The well distribution of functional small molecules is directed by the ordering of morphological block copolymer host matrix that allows for hybrid nanocomposite electret toward the application on nonvolatile memory devices.

CONCLUSIONS

In summary, the charge-trapping effects of nanocomposite electret in nonvolatile OFETs memories system compromising solution-processable FM small molecules selectively hydrogen-bonded with pyridine in PS-*b*-P4VP block copolymers to yield supramolecular structures were investigated. The memory characteristics based on nanoscale hybrid block copolymers/FM charge-trapping elements can be manipulated by changing the loading of FM and weight ratio of constituent blocks in block copolymers. By virtue of the morphological transition from the supramolecular interaction, the resulting memory performance can be facilely controlled. Furthermore, at least three well-separated data levels with enough sensing margin, ambipolar charge-trapping capability and high-density storage devices through the hybrid nanocomposite electret for nonvolatile OFETs memory device can be of great importance for scale-down devices, and the simplicity in material design and device fabrication can be compatible with integrated circuit technologies.

ASSOCIATED CONTENT

Supporting Information

2D GISAXS pattern, GISAXS profile, output curves, and statistics on electrical memory properties. This material is available free of charge via the Internet at http://pubs.acs.org.

AUTHOR INFORMATION

Corresponding Authors

*E-mail: shtung@ntu.edu.tw. (S.-H.T.)
*E-mail: clliu@ncu.edu.tw. (C.-L.L.)

Notes

The authors declare no competing financial interest.

ACKNOWLEDGMENTS

The authors acknowledge the financial support from Ministry of Science and Technology of Taiwan.

REFERENCES

(1) Ling, M. M.; Bao, Z. N. Thin Film Deposition, Patterning, and Printing in Organic Thin Film Transistors. *Chem. Mater.* **2004**, *16*, 4824–4840.
(2) Facchetti, A.; Yoon, M. H.; Marks, T. J. Gate Dielectrics for Organic Field-Effect Transistors: New Opportunities for Organic Electronics. *Adv. Mater.* **2005**, *17*, 1705–1725.
(3) Zaumseil, J.; Sirringhaus, H. Electron and Ambipolar Transport in Organic Field-Effect Transistors. *Chem. Rev.* **2007**, *107*, 1296–1323.
(4) Arias, A. C.; MacKenzie, J. D.; McCulloch, I.; Rivnay, J.; Salleo, A. Materials and Applications for Large Area Electronics: Solution-Based Approaches. *Chem. Rev.* **2010**, *110*, 3–24.
(5) Wu, W.; Liu, Y.; Zhu, D. Pi-Conjugated Molecules with Fused Rings for Organic Field-Effect Transistors: Design, Synthesis and Applications. *Chem. Soc. Rev.* **2010**, *39*, 1489–1502.
(6) Wang, C.; Dong, H.; Hu, W.; Liu, Y.; Zhu, D. Semiconducting pi-Conjugated Systems in Field-Effect Transistors: A Material Odyssey of Organic Electronics. *Chem. Rev.* **2012**, *112*, 2208–2267.
(7) Di, C.-a.; Zhang, F.; Zhu, D. Multi-Functional Integration of Organic Field-Effect Transistors (OFETs): Advances and Perspectives. *Adv. Mater.* **2013**, *25*, 313–330.
(8) Ling, Q.-D.; Liaw, D.-J.; Zhu, C.; Chan, D. S.-H.; Kang, E.-T.; Neoh, K.-G. Polymer Electronic Memories: Materials, Devices and Mechanisms. *Prog. Polym. Sci.* **2008**, *33*, 917–978.
(9) Heremans, P.; Gelinck, G. H.; Muller, R.; Baeg, K.-J.; Kim, D.-Y.; Noh, Y.-Y. Polymer and Organic Nonvolatile Memory Devices. *Chem. Mater.* **2011**, *23*, 341–358.
(10) Leong, W. L.; Mathews, N.; Tan, B.; Vaidyanathan, S.; Doetz, F.; Mhaisalkar, S. Towards Printable Organic Thin Film Transistor Based Flash Memory Devices. *J. Mater. Chem.* **2011**, *21*, 5203–5214.
(11) Chou, Y.-H.; Chang, H.-C.; Liu, C.-L.; Chen, W.-C. Polymeric Charge Storage Electrets for Non-volatile Organic Field Effect Transistor Memory Devices. *Polym. Chem.* **2015**, *6*, 341–352.
(12) Guo, Y.; Yu, G.; Liu, Y. Functional Organic Field-Effect Transistors. *Adv. Mater.* **2010**, *22*, 4427–4447.
(13) Naber, R. C. G.; Asadi, K.; Blom, P. W. M.; de Leeuw, D. M.; de Boer, B. Organic Nonvolatile Memory Devices Based on Ferroelectricity. *Adv. Mater.* **2010**, *22*, 933–945.
(14) Dhar, B. M.; Oezguen, R.; Dawidczyk, T.; Andreou, A.; Katz, H. E. Threshold Voltage Shifting for Memory and Tuning in Printed Transistor Circuits. *Mater. Sci. Eng., R* **2011**, *72*, 49–80.
(15) Lee, J.-S. Progress in Non-volatile Memory Devices Based on Nanostructured Materials and Nanofabrication. *J. Mater. Chem.* **2011**, *21*, 14097–14112.
(16) Han, S.-T.; Zhou, Y.; Roy, V. A. L. Towards the Development of Flexible Non-Volatile Memories. *Adv. Mater.* **2013**, *25*, 5425–5449.

DOI: 10.1021/acsami.5b00338
ACS Appl. Mater. Interfaces 2015, 7, 5663–5673

(17) Baeg, K.-J.; Noh, Y.-Y.; Ghim, J.; Kang, S.-J.; Lee, H.; Kim, D.-Y. Organic Non-volatile Memory Based on Pentacene Field-Effect transistors Using a Polymeric Gate Electret. *Adv. Mater.* **2006**, *18*, 3179−3183.
(18) Baeg, K.-J.; Noh, Y.-Y.; Ghim, J.; Lim, B.; Kim, D.-Y. Polarity Effects of Polymer Gate Electrets on Non-Volatile Organic Field-Effect Transistor Memory. *Adv. Funct. Mater.* **2008**, *18*, 3678−3685.
(19) Chiu, Y.-C.; Liu, C.-L.; Lee, W.-Y.; Chen, Y.; Kakuchi, T.; Chen, W.-C. Multilevel Nonvolatile Transistor Memories Using a Star-shaped Poly((4-diphenylamino)benzyl methacrylate) Gate Electret. *NPG Asia Mater.* **2013**, *5*, e35.
(20) Baeg, K.-J.; Khim, D.; Kim, J.; Yang, B.-D.; Kang, M.; Jung, S.-W.; You, I.-K.; Kim, D.-Y.; Noh, Y.-Y. High-Performance Top-Gated Organic Field-Effect Transistor Memory using Electrets for Monolithic Printed Flexible NAND Flash Memory. *Adv. Funct. Mater.* **2012**, *22*, 2915−2926.
(21) Chou, Y.-H.; Chiu, Y.-C.; Chen, W.-C. High-k Polymer-Graphene Oxide Dielectrics for Low-voltage Flexible Nonvolatile Transistor Memory Devices. *Chem. Commun.* **2014**, *50*, 3217−3219.
(22) Chen, C. M.; Liu, C. M.; Tsai, M. C.; Chen, H. C.; Wei, K. H. A Nanostructured Micellar Diblock Copolymer Layer Affects the Memory Characteristics and Packing of Pentacene Molecules in Non-volatile Organic Field-Effect Transistor Memory Devices. *J. Mater. Chem. C* **2013**, *1*, 2328−2337.
(23) Chou, Y.-H.; Yen, H.-J.; Tsai, C.-L.; Lee, W.-Y.; Liou, G.-S.; Chen, W.-C. Nonvolatile Transistor Memory Devices Using High Dielectric Constant Polyimide Electrets. *J. Mater. Chem. C* **2013**, *1*, 3235−3243.
(24) Chou, Y.-H.; You, N.-H.; Kurosawa, T.; Lee, W.-Y.; Higashihara, T.; Ueda, M.; Chen, W.-C. Thiophene and Selenophene Donor-Acceptor Polyimides as Polymer Electrets for Nonvolatile Transistor Memory Devices. *Macromolecules* **2012**, *45*, 6946−6956.
(25) Yu, A.-D.; Kurosawa, T.; Ueda, M.; Chen, W.-C. Polycyclic Arene-Based D-A Polyimide Electrets for High-Performance n-Type Organic Field Effect Transistor Memory Devices. *J. Polym. Sci. Polym. Chem.* **2014**, *52*, 139−147.
(26) Chiu, Y.-C.; Otsuka, I.; Halila, S.; Borsali, R.; Chen, W.-C. High-Performance Nonvolatile Transistor Memories of Pentacence Using the Green Electrets of Sugar-based Block Copolymers and Their Supramolecules. *Adv. Funct. Mater.* **2014**, *24*, 4240−4249.
(27) Wu, W.; Zhang, H.; Wang, Y.; Ye, S.; Guo, Y.; Di, C.; Yu, G.; Zhu, D.; Liu, Y. High-Performance Organic Transistor Memory Elements with Steep Flanks of Hysteresis. *Adv. Funct. Mater.* **2008**, *18*, 2593−2601.
(28) Bae, I.; Hwang, S. K.; Kim, R. H.; Kang, S. J.; Park, C. Wafer-Scale Arrays of Nonvolatile Polymer Memories with Microprinted Semiconducting Small Molecule/Polymer Blends. *ACS Appl. Mater. Interfaces* **2013**, *5*, 10696−10704.
(29) Hwang, S. K.; Choi, J. R.; Bae, I.; Hwang, I.; Cho, S. M.; Huh, J.; Park, C. High-Temperature Operating Non-volatile Memory of Printable Single-Wall Carbon Nanotubes Self-Assembled with a Conjugate Block Copolymer. *Small* **2013**, *9*, 831−837.
(30) Black, C. T.; Ruiz, R.; Breyta, G.; Cheng, J. Y.; Colburn, M. E.; Guarini, K. W.; Kim, H. C.; Zhang, Y. Polymer Self Assembly in Semiconductor Microelectronics. *IBM J. Res. Dev.* **2007**, *51*, 605−633.
(31) Leong, W. L.; Mathews, N.; Mhaisalkar, S.; Lam, Y. M.; Chen, T.; Lee, P. S. Micellar Poly(styrene-b-4-vinylpyridine)-Nanoparticle Hybrid System for Non-volatile Organic Transistor Memory. *J. Mater. Chem.* **2009**, *19*, 7354−7361.
(32) De Rosa, C.; Auriemma, F.; Di Girolamo, R.; Pepe, G. P.; Napolitano, T.; Scaldaferri, R. Enabling Strategies in Organic Electronics Using Ordered Block Copolymer Nanostructures. *Adv. Mater.* **2010**, *22*, 5414−5419.
(33) Lee, J.-S.; Kim, Y.-M.; Kwon, J.-H.; Sim, J. S.; Shin, H.; Sohn, B.-H.; Jia, Q. Multilevel Data Storage Memory Devices Based on the Controlled Capacitive Coupling of Trapped Electrons. *Adv. Mater.* **2011**, *23*, 2064−2068.
(34) Chen, J.-C.; Liu, C.-L.; Sun, Y.-S.; Tung, S.-H.; Chen, W.-C. Tunable Electrical Memory Characteristics by the Morphology of Self-Assembled Block Copolymers:PCBM Nanocomposite Films. *Soft Matter* **2012**, *8*, 526−535.
(35) Yu, A.-D.; Liu, C.-L.; Chen, W.-C. Supramolecular Block Copolymers: Graphene Oxide Composites for Memory Device Applications. *Chem. Commun.* **2012**, *48*, 383−385.
(36) Lian, S.-L.; Liu, C.-L.; Chen, W.-C. Conjugated Fluorene Based Rod-Coil Block Copolymers and Their PCBM Composites for Resistive Memory Switching Devices. *ACS Appl. Mater. Interfaces* **2011**, *3*, 4504−4511.
(37) Liu, J.; Gu, P.; Zhou, F.; Xu, Q.; Lu, J.; Li, H.; Wang, L. Preparation of TCPP: Block Copolymer Composites and Study of Their Memory Behavior by Tuning the Loading Ratio of TCPP in the Polymer Matrix. *J. Mater. Chem. C* **2013**, *1*, 3947−3954.
(38) Ahn, B.; Kim, D. M.; Hsu, J.-C.; Ko, Y.-G.; Shin, T. J.; Kim, J.; Chen, W.-C.; Ree, M. Tunable Film Morphologies of Brush-Linear Diblock Copolymer Bearing Difluorene Moieties Yield a Variety of Digital Memory Properties. *ACS Macro Lett.* **2013**, *2*, 555−560.
(39) Kang, N.-G.; Cho, B.; Kang, B.-G.; Song, S.; Lee, T.; Lee, J.-S. Structural and Electrical Characterization of a Block Copolymer-Based Unipolar Nonvolatile Memory Device. *Adv. Mater.* **2012**, *24*, 385−390.
(40) Chen, C.-M.; Liu, C.-M.; Wei, K.-H.; Jeng, U. S.; Su, C.-H. Non-volatile Organic Field-Effect Transistor Memory Comprising Sequestered Metal Nanoparticles in a Diblock Copolymer Film. *J. Mater. Chem.* **2012**, *22*, 454−461.
(41) Wei, Q.; Lin, Y.; Anderson, E. R.; Briseno, A. L.; Gido, S. P.; Watkins, J. J. Additive-Driven Assembly of Block Copolymer-Nanoparticle Hybrid Materials for Solution Processable Floating Gate Memory. *ACS Nano* **2012**, *6*, 1188−1194.
(42) Zhu, H.; Hacker, C. A.; Pookpanratana, S. J.; Richter, C. A.; Yuan, H.; Li, H.; Kirillov, O.; Ioannou, D. E.; Li, Q. Non-volatile Memory with Self-assembled Ferrocene Charge Trapping Layer. *Appl. Phys. Lett.* **2013**, *103*, 053102.
(43) Kuila, B. K.; Rama, M. S.; Stamm, M. Supramolecular Assembly of Poly(styrene)-*b*-poly(4-vinylpyridine) and Ferroceneacetic Acid: An Easy Way to Large-Scale Controllable Periodic Arrays of Iron Oxide Nanomaterials. *Adv. Mater.* **2011**, *23*, 1797−1800.
(44) Rancatore, B. J.; Mauldin, C. E.; Tung, S.-H.; Wang, C.; Hexemer, A.; Strzalka, J.; Frechet, J. M. J.; Xu, T. Nanostructured Organic Semiconductors via Directed Supramolecular Assembly. *ACS Nano* **2010**, *4*, 2721−2729.
(45) Tung, S.-H.; Kalarickal, N. C.; Mays, J. W.; Xu, T. Hierarchical Assemblies of Block-Copolymer-Based Supramolecules in Thin Films. *Macromolecules* **2008**, *41*, 6453−6462.
(46) Tung, S.-H.; Xu, T. Templated Assembly of Block Copolymer toward Nonequilibrium Nanostructures in Thin Films. *Macromolecules* **2009**, *42*, 5761−5765.
(47) van Zoelen, W.; Asumaa, T.; Ruokolainen, J.; Ikkala, O.; ten Brinke, G. Phase Behavior of Solvent Vapor Annealed Thin Films of PS-*b*-P4VP(PDP) Supramolecules. *Macromolecules* **2008**, *41*, 3199−3208.
(48) Roland, S.; Gaspard, D.; Prud'homme, R. E.; Bazuin, C. G. Morphology Evolution in Slowly Dip-Coated Supramolecular PS-b-P4VP Thin Films. *Macromolecules* **2012**, *45*, 5463−5476.
(49) Zhou, Y.; Han, S.-T.; Sonar, P.; Roy, V. A. L. Nonvolatile Multilevel Data Storage Memory Device from Controlled Ambipolar Charge Trapping Mechanism. *Sci. Rep.* **2013**, *3*, 2319.
(50) Debucquoy, M.; Rockele, M.; Genoe, J.; Gelinck, G. H.; Heremans, P. Charge Trapping in Organic Transistor Memories: On the Role of Electrons and Holes. *Org. Electron.* **2009**, *10*, 1252−1258.
(51) Chang, H.-C.; Lu, C.; Liu, C.-L.; Chen, W.-C. Single-Crystal C60 Needle/CuPc Nanoparticle Double Floating-Gate for Low-Voltage Organic Transistors Based Non-Volatile Memory Devices. *Adv. Mater.* **2015**, *27*, 27−33.
(52) Suga, T.; Takeuchi, S.; Nishide, H. Morphology-Driven Modulation of Charge Transport in Radical/Ion-Containing, Self-Assembled Block Copolymer Platform. *Adv. Mater.* **2011**, *23*, 5545−5549.
(53) Suga, T.; Sakata, M.; Aoki, K.; Nishide, H. Synthesis of Pendant Radical- and Ion-Containing Block Copolymers via Ring-Opening

DOI: 10.1021/acsami.5b00338
ACS Appl. Mater. Interfaces 2015, 7, 5663−5673

Metathesis Polymerization for Organic Resistive Memory. *ACS Macro Lett.* **2014**, *3*, 703−707.
(54) Kim, K.; Kim, Y. Y.; Park, S.; Ko, Y.-G.; Rho, Y.; Kwon, W.; Shin, T. J.; Kim, J.; Ree, M. Nanostructure- and Orientation-Controlled Digital Memory Behaviors of Linear-Brush Diblock Copolymers in Nanoscale Thin Films. *Macromolecules* **2014**, *47*, 4397−4407.

DOI: 10.1021/acsami.5b00338
ACS Appl. Mater. Interfaces 2015, 7, 5663−5673